

Hole Hopping Across a Protein-Protein Interface

Kana Takematsu,^a Petr Pospíšil,^b Martin Pižl,^{b,c} Michael Towrie,^d Jan Heyda,^{b,c} Stanislav Záliš,^b
Jens T. Kaiser,^e Jay R. Winkler,^{e,*} Harry B. Gray,^{e,*} Antonín Vlček,^{b,f,*}

^a Department of Chemistry, Bowdoin College, Brunswick, ME 04011, USA

^b J. Heyrovský Institute of Physical Chemistry, Academy of Sciences of the Czech Republic,
Dolejškova 3, CZ-182 23 Prague, Czech Republic

^c University of Chemistry and Technology, Prague, Technická 5, CZ-166 28 Prague, Czech
Republic

^d Central Laser Facility, Research Complex at Harwell, Science and Technology Facilities Council,
Rutherford Appleton Laboratory, Harwell Oxford, Didcot, Oxfordshire, OX11 0FA, UK

^e Beckman Institute, California Institute of Technology, Pasadena, CA 91125, USA

^f Queen Mary University of London, School of Biological and Chemical Sciences, Mile End Road,
London E1 4NS, United Kingdom

Supporting Information

Contents:

S1. Structures	p. S2
S2. Luminescence decay	p. S5
S3. Time-resolved IR spectroscopy and mechanisms	p. S9
S4. Representative kinetics fits	p. S14
References	p. S18

Section S1: Structures

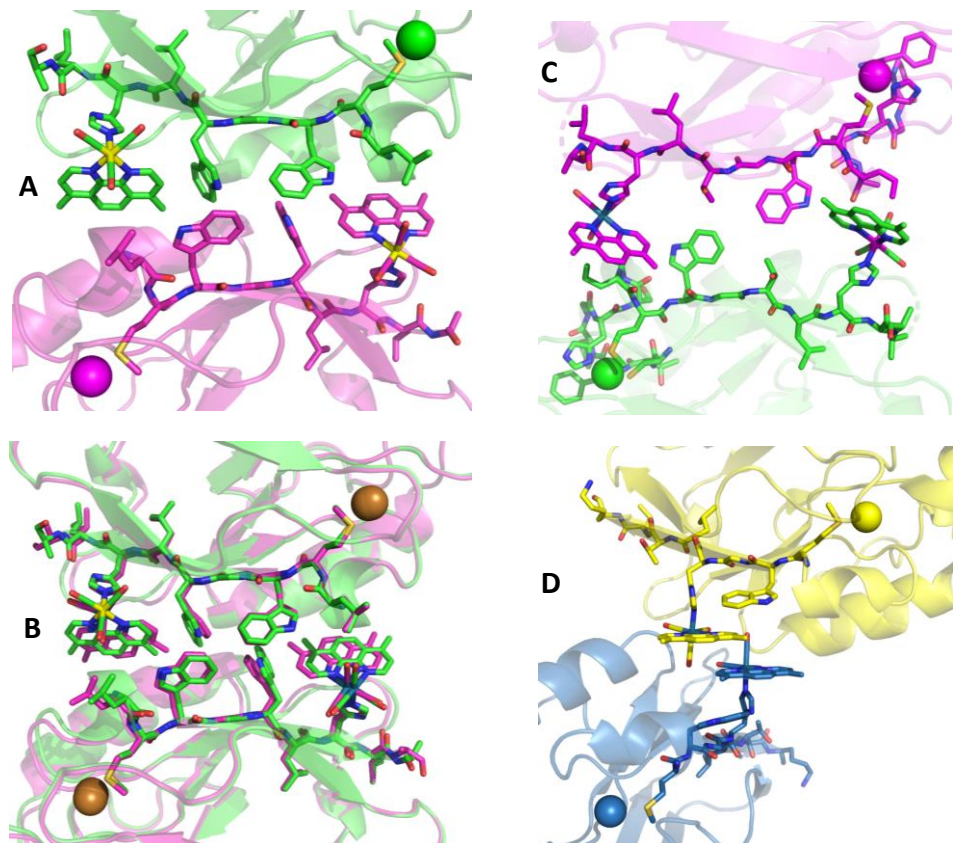


Figure S1. Structures of the protein-protein interfacial regions of $\text{Re126WWCu}^{\text{II}}$ (A), $\text{Re126WWCu}^{\text{II}}$ and $\text{Re126FWCu}^{\text{II}}$ in superposition (B), $\text{Re126TWCu}^{\text{II}}$ (ref.¹) (C), and $\text{Re124W122Cu}^{\text{II}}$ (D). In $\{\text{Re124W122Cu}^{\text{II}}\}_2$, the dmp ligands are separated by 4.5 Å; and the shortest *intermolecular* dmp-W122' distance is 7.1 Å.

Table S1. Shortest atom-atom intramolecular distances between redox-active sites.² (Only aromatic C and N atoms, as well as Re and Cu are considered. Values averaged over the molecules comprising the asymmetric unit.)

Distance	Re126FWCu ^{II}	Re126WWCu ^{II}	Re126WFCu ^{II} ^a	Re124W122Cu ^{II} ^g
Re–W124	-	6.9	7.6	-
dmp–W124	-	3.5 ^b	3.7 ^c	-
W124–W122	-	3.9 ^d	-	-
Re–W122	11.1	11.4	-	6.3
dmp–W122	7.1	7.8	-	3.4
Cu–W122	10.7	10.7	15.7 ^e	10.8
Cu–dmp	20.2	20.6	19.9	16.0 ^f
Cu–Re	23.3	22.9	22.7	19.4
Angle (°)				
dmp–W124	-	67.7		20.8 ^h
W124–W122	-	78.7		-

^a Two molecules with different Re/W122-indole orientations are present. The listed distances are pertinent to the molecule with closer contacts. ^b An additional close contact (3.9 Å) exists between the W124 indole ring and C(CH₃-dmp). ^c Closest distance between the indole ring and C(CH₃-dmp) = 3.5 Å. ^d The distances in the four molecules comprising the asymmetric cell are in the range 3.6–4.1 Å. ^e Cu–W124 distance. ^f Closest distance between Cu and C(CH₃-dmp) = 15.3 Å. ^g PDB: 2I7O, see Figure S1. ^h dmp–W122

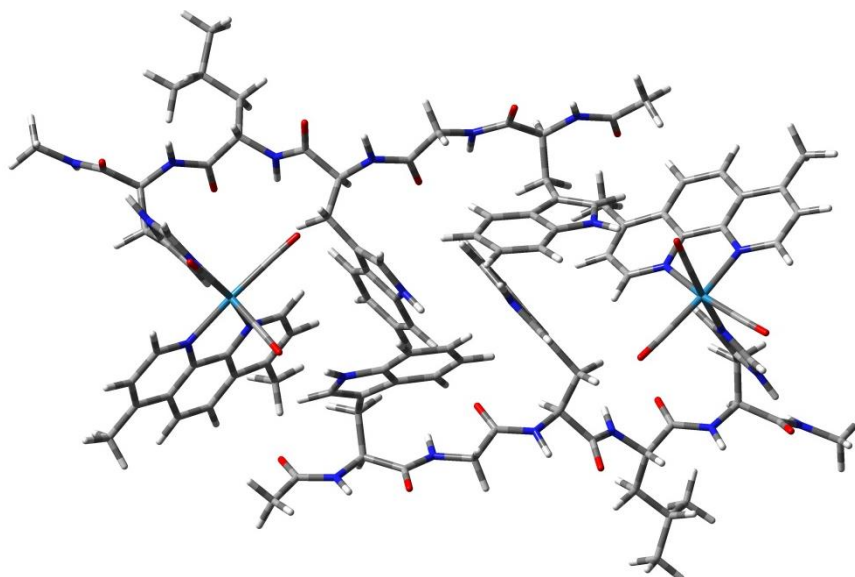


Figure S2. DFT (PBE0-D3) optimized structure of {Re(CO)₃(dmp)H126A125W124G123W122}₂ in a water dielectric continuum.

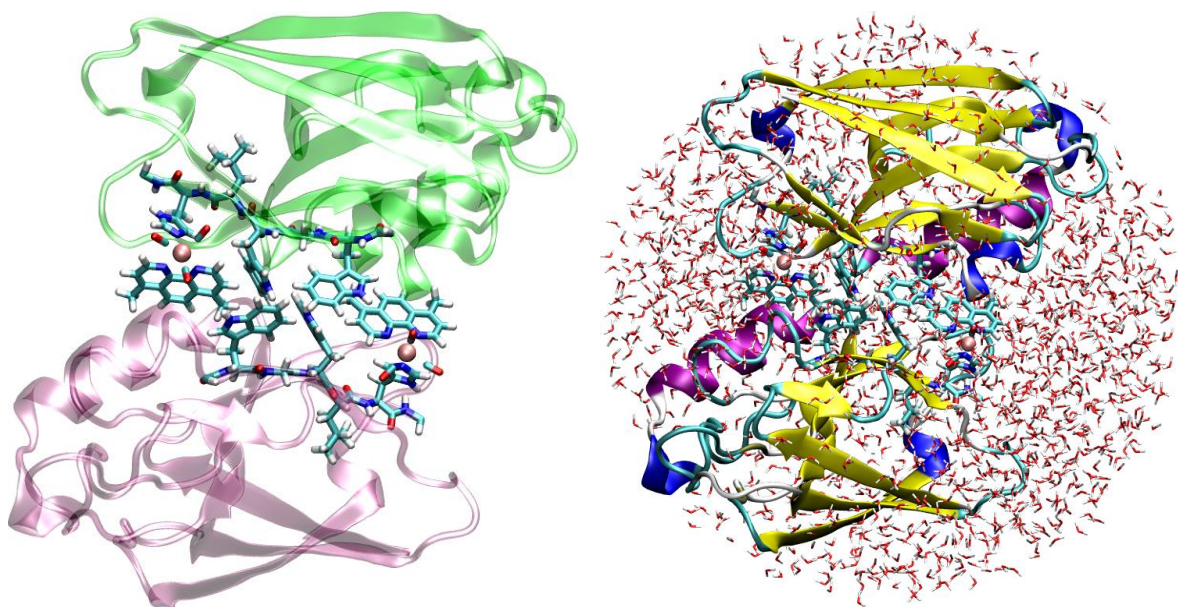


Figure S3. QM/MM optimized structure of $\{\text{Re126WWCu}\}_2$ solvated with 2088 explicit water molecules. Shown without (left) and with surrounding water (right).

Table S2. Experimental and calculated shortest atom-atom *intermolecular* distances between redox cofactors of $\{\text{Re126WWCu}\}_2$. (Only aromatic C and N atoms, as well as Re and Cu are considered. Experimental values from Table 1.)

Distance (Å)	Experiment $\{\text{Re126WWCu}\}_2$	QM/MM $\{\text{Re126WWCu}\}_2$	DFT model ^a
Re-W122'	7.0	6.5	4.7
dmp-W122'	3.8	3.5	4.4
W124-W122'	3.3	3.4	3.5
W124-W124'	3.5-4.8 ^b	3.3	3.2
W122-W122'	3.7	3.5	3.8
Angle (°)			
dmp-W122'	15.1-10.6	19.7	26.8
W124-W122'	84.4-68.1 ^b	73.7	57.7
W124-W124'	4.3-17.6 ^c	6.7	19.8

^a Bare $\{\text{Re}(\text{CO})_3(\text{dmp})\text{H126L125W124G123W122}\}_2$ in a water dielectric-continuum shown in Figure S2. ^b 3.5/4.8 Å and 84.4/68.1° correspond to B-C/A-D interfaces. ^c 4.3/17.6 correspond to B-C/A-D interfaces.

S2. Luminescence decay

S2.1. Re126FWCu^{II}

Luminescence decay of **Re126FWCu^{II}** was measured in two sets of experiments: one in the 12-198 μM concentration range using ~ 8 ns, 355 nm laser excitation and PMT detection that produced tri-exponential (~ 50 , ~ 300 ns, and low-amplitude ~ 1.1 μs) decay kinetics. The minor ~ 1.1 μs component is likely due to contamination with the Cu^{I} form. In analogy with previously studied **{Re126TWCu^{II}}₂**,¹ the ~ 50 and ~ 300 ns decays are attributed to *Re luminescence from dimers, where it undergoes *intermolecular* ET quenching, and from unreactive monomers, respectively. The second set of measurements was carried out on more concentrated samples (0.3-1.2 mM) using ~ 80 ps, 373 nm pulses and TCSPC detection. These experiments were carried out in three different time ranges: 0-50 (7.07 ps/channel), 0-100 (57.25 ps/channel), and 0-1000 ns (486 ps/channel). These measurements showed multiexponential pico- and nanosecond decays. (The ~ 1 μs component was absent.) The data are summarized in Tables S2-4. (Amplitudes are defined as normalized pre-exponential factors. IRF iterative deconvolution with a multiexponential fitting model was used for all data obtained.)

To demonstrate the dimerization equilibrium between ET-inactive **Re126FWCu^{II}** monomer (~ 300 ns) and reactive dimer (~ 50 ns and shorter components), we have combined the two sets of measurements and analyzed the decay kinetics in a compatible way. Figure 2 shows the concentration dependence of the amplitude of the shorter decay component(s) (that is equal to the dimer fraction, see the SI of ref.¹). Its gradual asymptotic increase with increasing concentration demonstrates the presence of the equilibrium. Comparison with the analogous behavior of **Re126TWCu^{II}**¹ indicates that replacing the 124 threonine by aromatic phenylalanine increases the dimerization constant from about 6×10^3 to roughly 1.6×10^4 M^{-1} .

Experiments with picosecond time resolution (Tables S4, S5) show that the luminescence decay is dominated by a ~ 50 ps component whose relative amplitude decreases from 64 to 56% when the detection wavelength is shifted from the high-energy side of the luminescence band (500 nm) to the band maximum (560 nm). Hence, the 50 ps decay is

affected by a dynamic Stokes shift that results from relaxation of the *Re chromophore and its environment.^{3,4} The amplitude decrease with dilution suggests that at least part of the relaxation is related to the dynamics of the protein-protein interface in the dimeric species namely hydration and mobility of protein segments in the vicinity of *Re (Table S4). The 500-600 ps and 5 ns decays are associated with redox equilibria of the dimeric species.

Table S3. *Re luminescence decay kinetics of **Re126FWCu^{II}** measured at 560 nm by TCSPC over a 0-1000 ns range (0.486 ns/channel). 3-exponential global fit with linked lifetimes. Measured in H₂O, 20 mM NaP_i, pH \cong 7.2.

Lifetime ns	Amplitude, %			
	1.2 mM	0.6 mM	0.4 mM	0.3 mM
~8	45	31	29	35
56.2	30	30	28	23
261	24	39	44	42

Table S4. *Re luminescence decay kinetics of 1.2 mM **Re126FWCu^{II}** measured at 500 and 560 nm by TCSPC over a 0-50 ns range (7.07 ps/channel). 4-exponential global fit with linked lifetimes. Measured in H₂O, 20 mM NaP_i, pH \cong 7.2.

Lifetime ns	Amplitudes, %	
	500 nm	560 nm
0.04	64	56
0.54	13	12
5.1	12	13
\geq 50	11	19

Table S5. *Re luminescence decay kinetics of **Re126FWCu^{II}** measured at 500 nm by TCSPC over a 0-50 ns range (7.07 ps/channel). 4-exponential global fit with linked lifetimes. Measured in H₂O, 20 mM NaP_i, pH \cong 7.2.

Lifetime ns	Amplitude, %	
	1.2 mM	0.4 mM
0.05	63	55
0.58	13	14
5.1	12	15
\geq 50	12	16

Re126WWCu^{II}**Table S6.** *Re luminescence decay kinetics of **Re126WWCu^{II}** measured at 500 and 560 nm. 4-exponential global fit with linked lifetimes for each excitation wavelength. TCSPC detection over a 0-50 ns range (7.07 ps/channel), H₂O, 20 mM NaP_i, pH \cong 7.2.

Lifetime ns	1.0 mM	0.3 mM
	500 nm	500 nm
0.06	56	51
0.31	38	42
4.2	3	4
>30	3	3
	560 nm	560 nm
0.12	56	59
0.45	29	28
6.8	7	6
>40	8	7

Table S7. *Re luminescence decay kinetics of **Re126WWCu^{II}** measured at 500, 560, and 600 nm using TCSPC detection over a 0-50 ns range (7.07 ps/channel). 4-exponential global fit with linked lifetimes for each concentration. Measured in H₂O, 20 mM NaP_i, pH \cong 7.2.

1.0 mM solution			
Lifetime ns	Amplitude, %		
	500 nm	560 nm	600 nm
0.06	56	41	43
0.32	38	44	42
4.7	3	6	5
>30	3	9	10
0.3 mM solution			
0.08	52	45	-
0.33	41	41	-
4.8	4	5	-
>40	3	8	-

Table S8. *Re luminescence decay kinetics of **Re126WFCu^{II}** measured at 560 nm by TCSPC over a 0-1000 ns range (0.486 ns/channel). 3-exponential global fit with linked lifetimes. Measured in H₂O, 20 mM NaP_i, pH \cong 7.2.

Lifetime ns	Amplitude, %	
	1.0 mM	0.3 mM
~11	58	45
66	31	46
311 ^a	11	9

^aThe minor 311 ns decay corresponds to the hundreds-of-nanosecond minor kinetics component observed by TRIR. It is likely related to intermolecular ET kinetics.

Re126WFCu^{II}

Table S9. *Re luminescence decay kinetics of 1.8 mM **Re126WFCu^{II}** measured at 500 and 560 nm and TCSPC detection over a 0-50 ns range (7.07 ps/channel). 4-exponential global fit with linked lifetimes. Measured in H₂O, 20 mM NaP_i, pH \cong 7.2.

Lifetime ns	Amplitude, %	
	500 nm	560 nm
0.05	69	54
0.27	23	29
4.14	4	6
~40	4	11

S3. Time-resolved IR spectroscopy and mechanisms

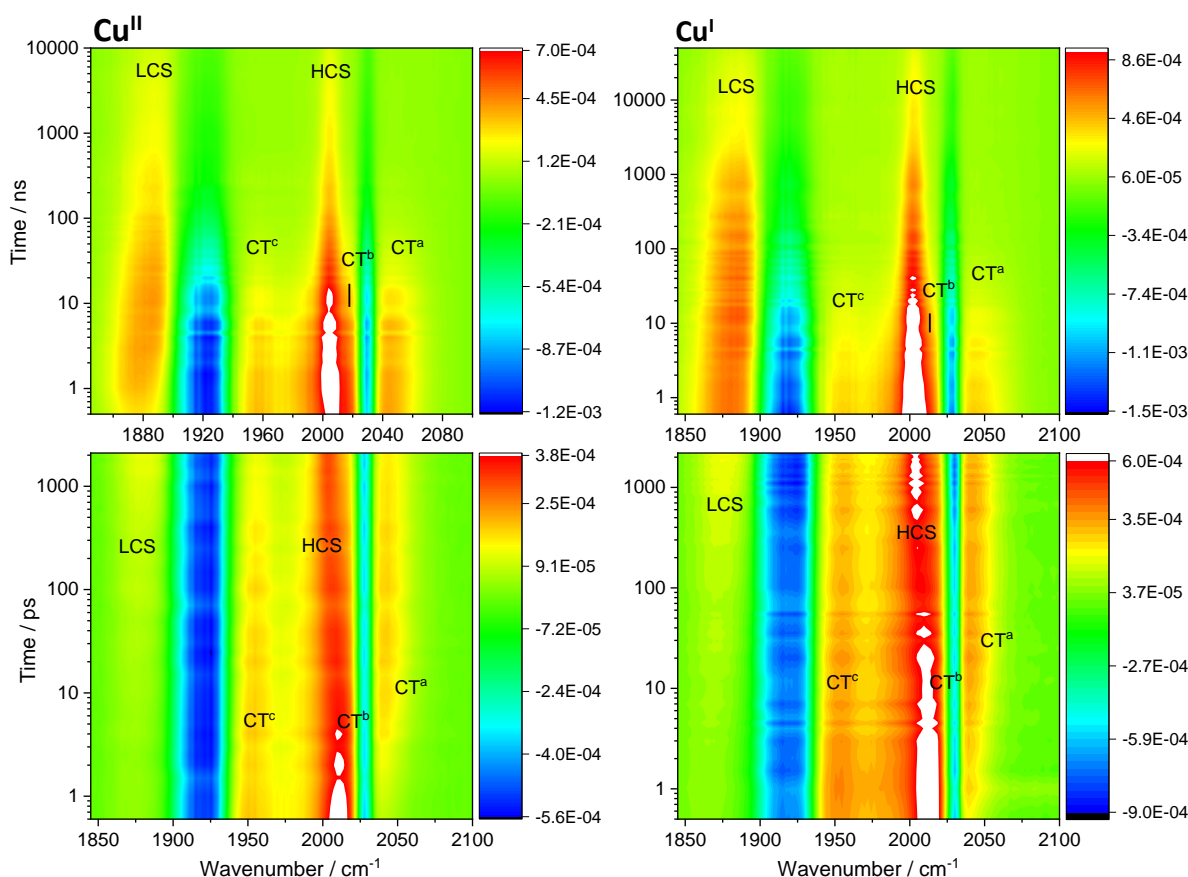


Figure S4. Difference TRIR spectra of **Re126WWCu^{II}** (left) and **Re126WWCu^I** (right). Negative (blue) features correspond to depleted ground-state population; positive features correspond to photogenerated transients (yellow-orange-red-white in the order of increasing intensity). Picosecond spectra (bottom) were measured in ~ 1.5 mM/ H_2O (Cu^{II}), and ~ 1.6 mM/ D_2O (Cu^{I}) solutions, 20 mM KP_i , pH ($\text{pD} \cong 7.1$) using 355 and 400 nm excitation, respectively. Spectra obtained at 0.5 ps show the ground-state bleach ($\sim 1922, 2030 \text{ cm}^{-1}$), features due to a hot CT state, and a weak LCS signal formed within the instrument time resolution. Nanosecond spectra were measured in ~ 1.5 mM/ H_2O (Cu^{II}), and ~ 1.3 mM/ H_2O , (Cu^{I}) solutions, 20 mM KP_i , pH $\cong 7.1$. Excited at 355 nm. Transient bands occur at: 1956 (CT^{II}), ~ 2014 (CT^{I}), 2043 (CT), 2004 cm^{-1} (HCS). The LCS bands shift from ~ 1873 (1 ps) to $\sim 1887 \text{ cm}^{-1}$ (10 ns) for Cu^{II} and from 1867 (1 ps) to $\sim 1883 \text{ cm}^{-1}$ (500 ns) for Cu^{I} . (Maxima values are only apparent as LCS overlaps with the bleach.) Similar spectra were obtained in a 0.5-1 mM concentration range.

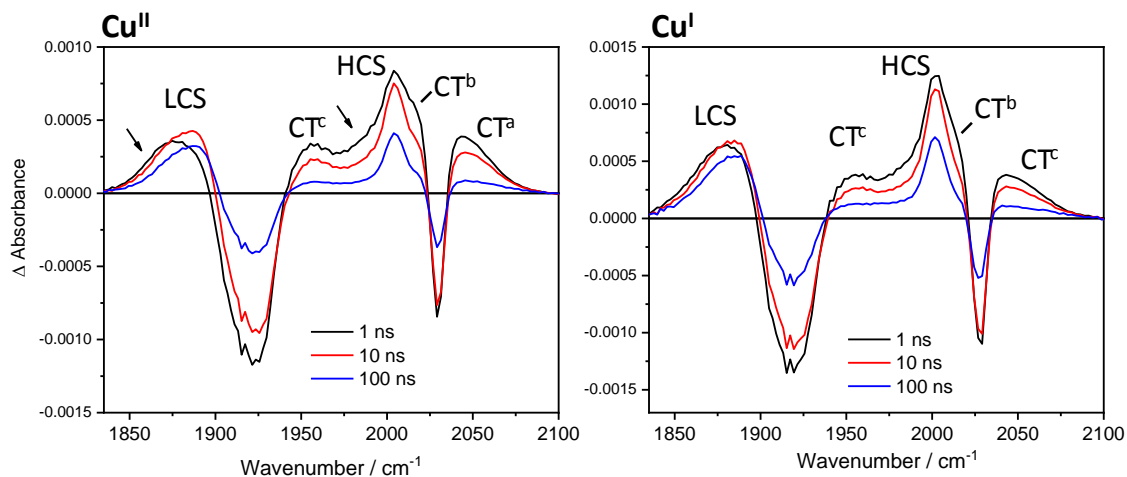


Figure S5. Difference nanosecond TRIR spectra of **Re126WWCu^{II}** (left) and **Re126WWCu^I** (right) measured at 1, 10, and 100 ns after 355 nm, 700 ps excitation. Arrows indicate early-time CS band broadening. (Narrowing of the LCS band between 1 and 10 ns is not apparent in the left panel because of a larger CS intensity rise.) Experimental conditions as in the top two panels of Figure S2.

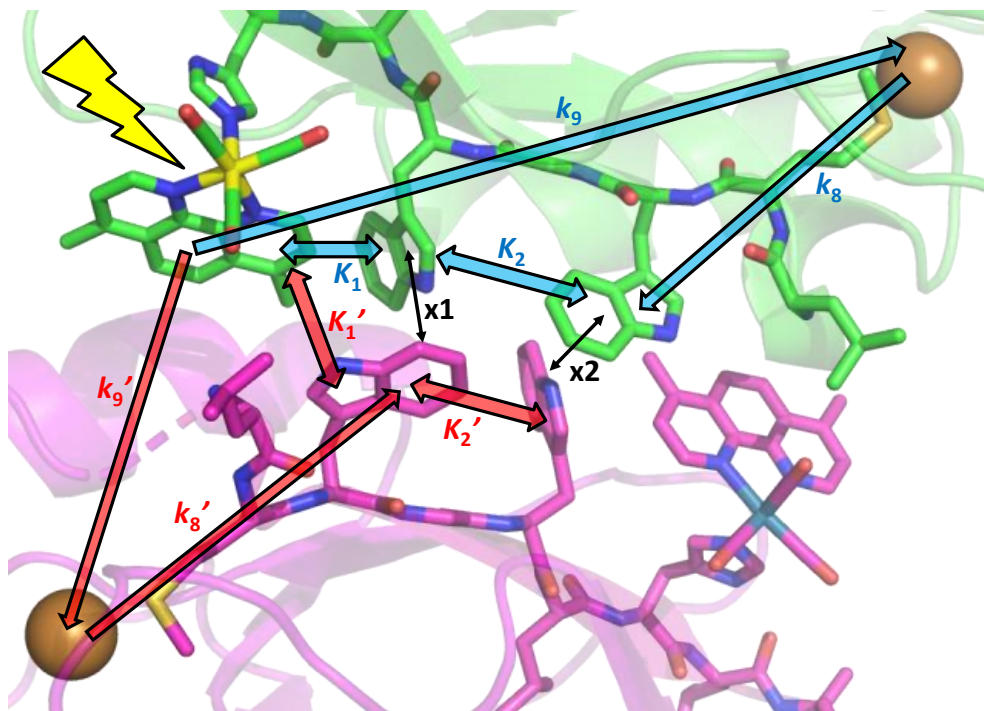


Figure S6. *Intra-* (blue) and *intermolecular* (red) ET processes in **{Re126WWCu^I}₂**.

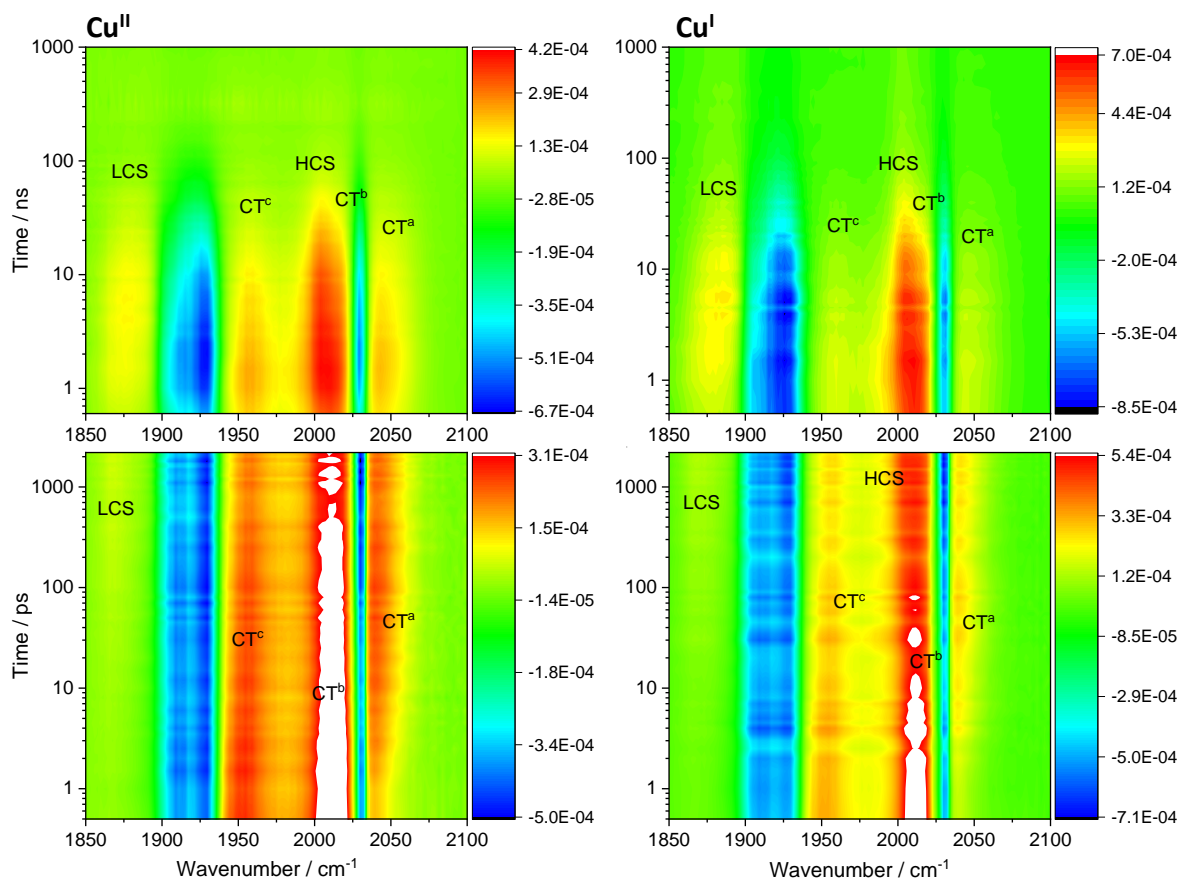


Figure S7. Difference TRIR spectra of **Re126WFCu^{II}** and **Re126WFCu^I**. Negative (blue) features correspond to depleted ground-state population; positive features correspond to photogenerated transients (yellow-orange-red-white in the order of increasing intensity). Picosecond spectra (bottom) were measured in 1.2 mM (Cu^{II}) and 1 mM (Cu^I) solutions in D₂O, 20 mM KP_i, pD \cong 7.1 using 400 nm, 50 fs excitation. Spectra obtained shortly after excitation (\leq 1ps) show the ground-state bleach, features due to a hot CT state and a weak CS signal formed within the instrument time resolution. Nanosecond spectra (top) were measured in 1.3 mM (Cu^{II}) and 0.8 mM (Cu^I) solutions in H₂O, 20 mM KP_i, pH \cong 7.1. Excited at 355 nm, 0.8 ns.

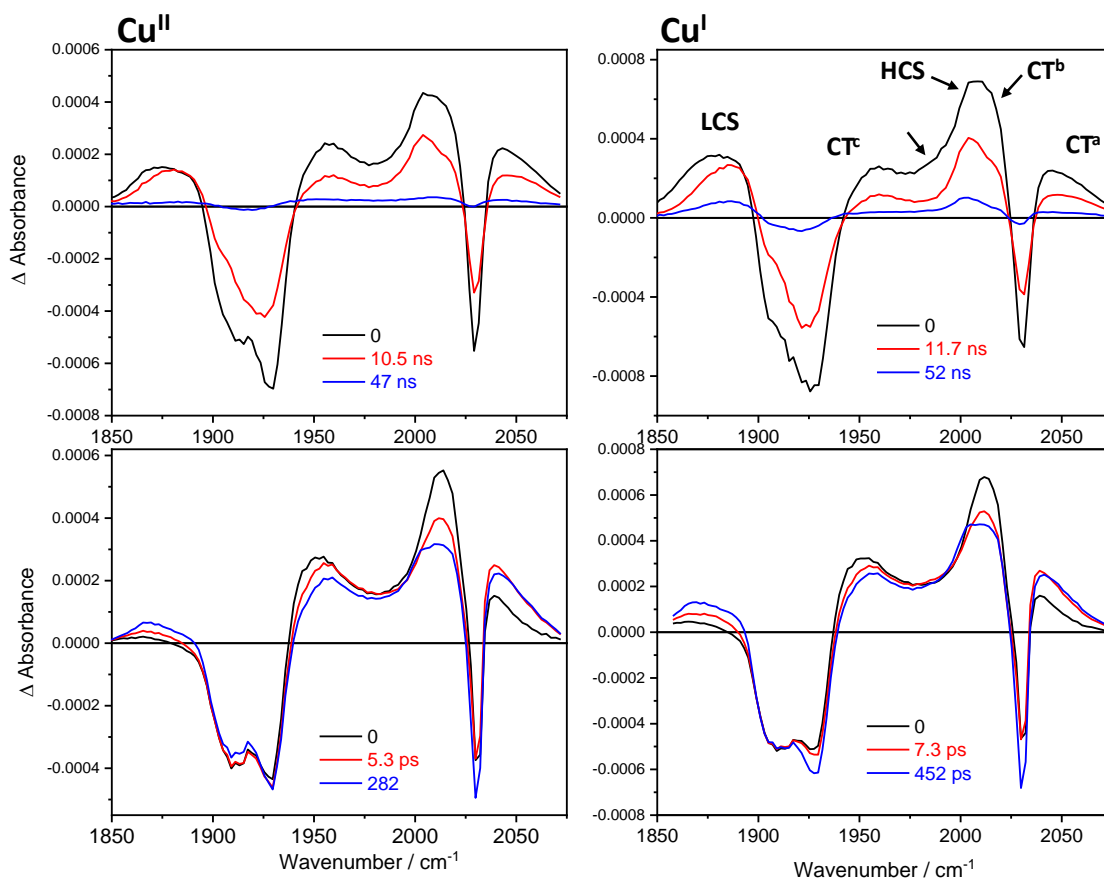


Figure S8. Evolution associated spectra of **Re126WFCu^{II}** (left) and **Re126WFCu^I** (right) obtained by global fit of picosecond (bottom) and nanosecond (top) 3D TRIR data (kinetic/spectral) using a sequential multiexponential model. Black curves are spectra extrapolated to time 0 and correspond to the species formed within the 355, ~ 0.7 ns laser pulse excitation. Red, blue and green curves correspond to spectra associated with the specified kinetics. The longest-lifetime spectra correspond to the residual species that remains after a process characterized by the specified time constant and decays on a timescale longer than the measurement. Band labelling in the top-right panel is valid for all spectra shown. The unlabeled arrow indicates decay of the LCS early-time broadening and of the ~ 1985 cm^{-1} shoulder. Experimental conditions as in Figure S7.

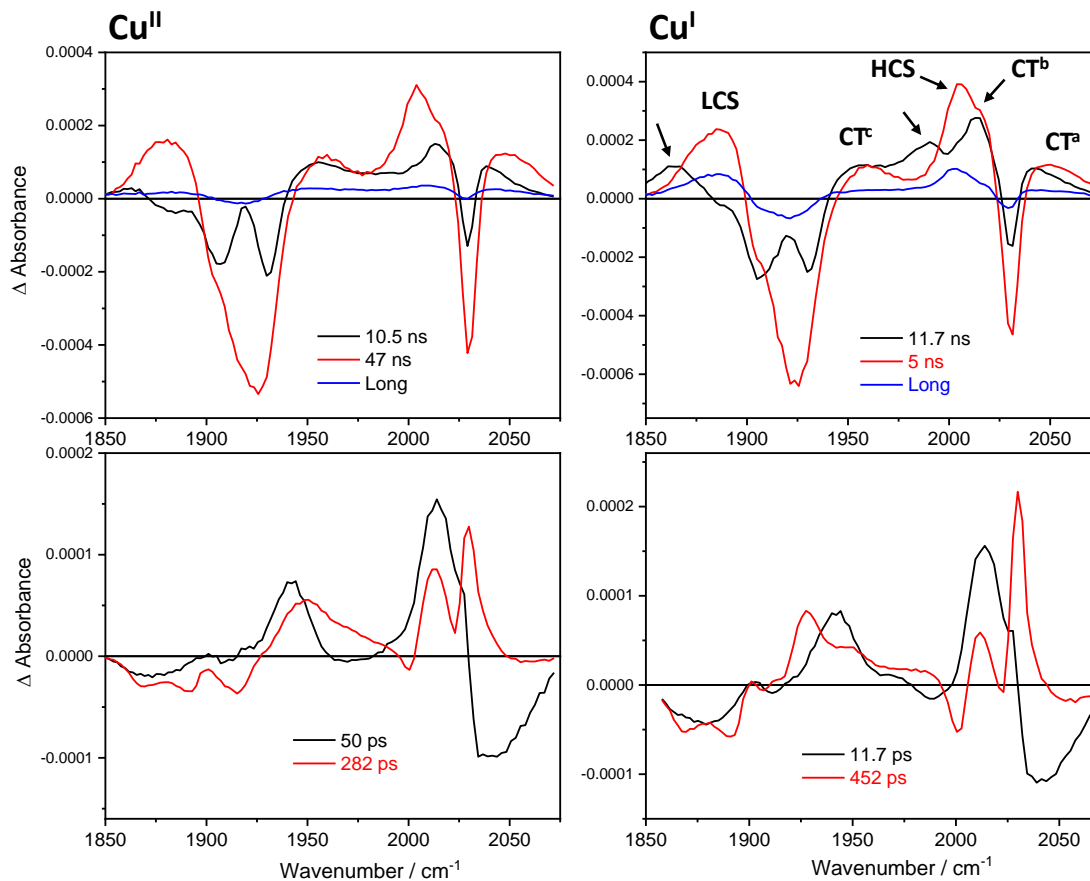


Figure S9. Decay associated spectra of $\text{Re126WFCu}^{\text{II}}$ (left) and $\text{Re126WFCu}^{\text{I}}$ (right) obtained by global fit of picosecond (bottom) and nanosecond (top) 3D TRIR data (kinetic/spectral) using a sequential multiexponential model. Negative and positive features correspond to signal rise and decay, respectively. Band labelling in the top-right panel is valid for all spectra shown. The unlabeled arrow indicates decay of the LCS early-time broadening and of the $\sim 1985 \text{ cm}^{-1}$ shoulder. Experimental conditions as in Figure S7.

S4. Representative kinetics fits

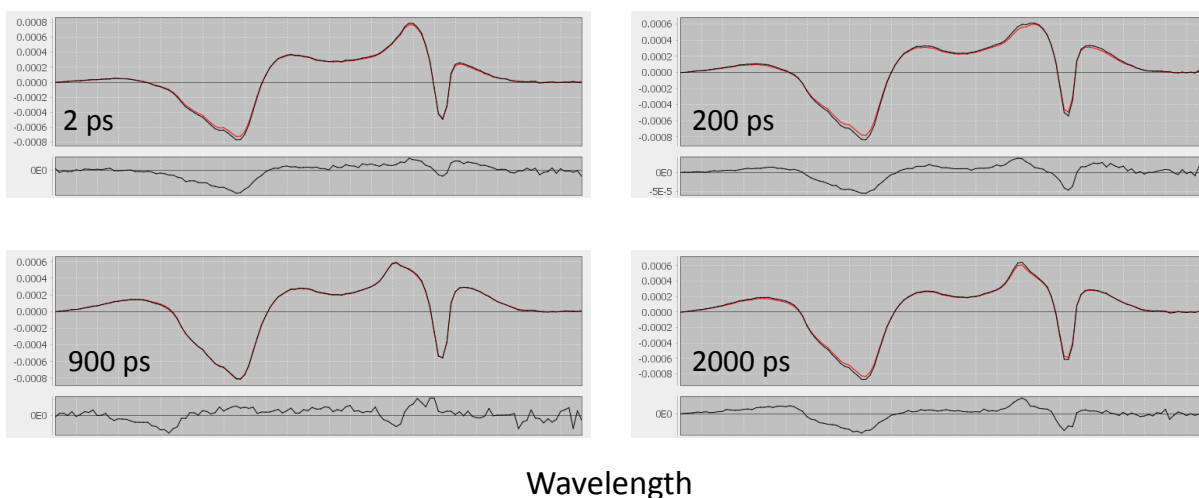


Figure S10. Experimental (black) and fitted (red) picosecond TRIR spectra of $\text{Re126FWCu}^{\text{I}}$ at selected time delays. Residuals are shown below the spectra. Conditions as in Figures 4 and 5. The x-axis is calibrated in detector pixels, corresponding to IR-probe wavelength.

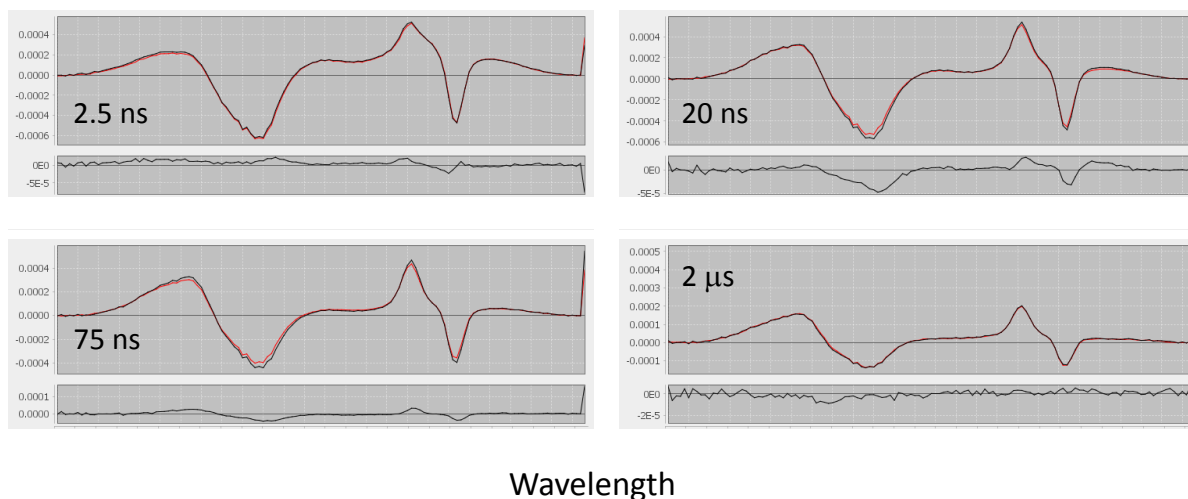


Figure S11. Experimental (black) and fitted (red) nanosecond TRIR spectra of $\text{Re126FWCu}^{\text{I}}$ at selected time delays. Residuals are shown below the spectra. Conditions as in Figures 4 and 5. The x-axis is calibrated in detector pixels, corresponding to IR-probe wavelength.

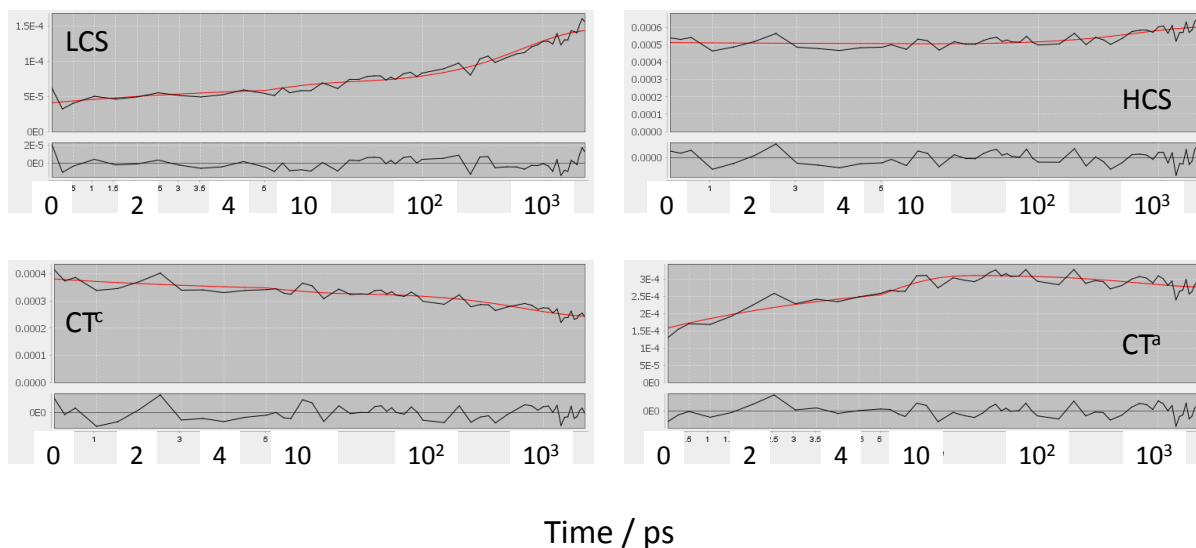


Figure S12. Experimental (black) and fitted (red) time profiles of picosecond TRIR differential absorbance of **Re126FWCu^I** measured at maxima of selected IR features. Residuals are shown below the profiles. Conditions as in Figures 4 and 5. The initial CT^a rise is due to relaxation. The first 5 ps are shown on a linear scale, the 5-2100 range is on a logarithmic scale.

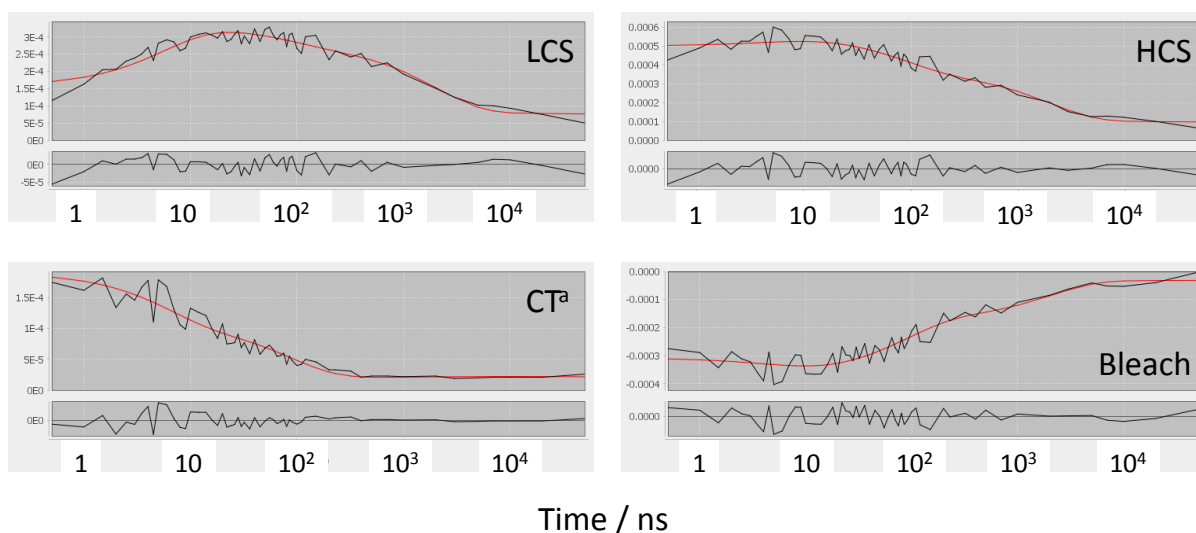


Figure S13. Experimental (black) and fitted (red) time profiles of nanosecond TRIR differential absorbance of **Re126FWCu^I** measured at maxima of selected IR features. Residuals are shown below the profiles. Conditions as in Figures 4 and 5. Bleach profile measured at 2028 cm^{-1} .

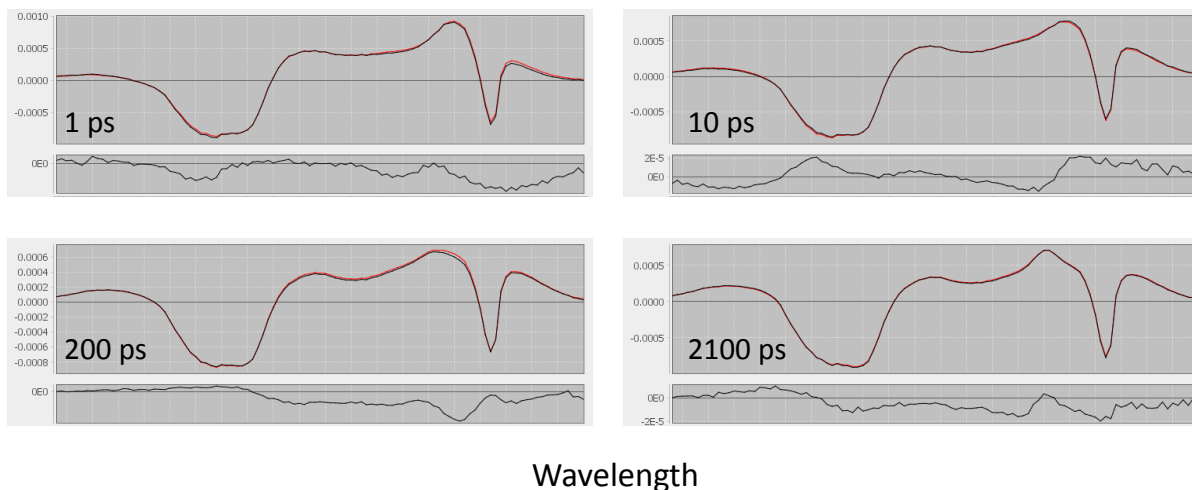


Figure S14. Experimental (black) and fitted (red) picosecond TRIR spectra of **Re126WWCu^I** at selected time delays. Residuals are shown below the spectra. Conditions as in Figures 6 and 7. The x-axis is calibrated in detector pixels, corresponding to IR-probe wavelength.

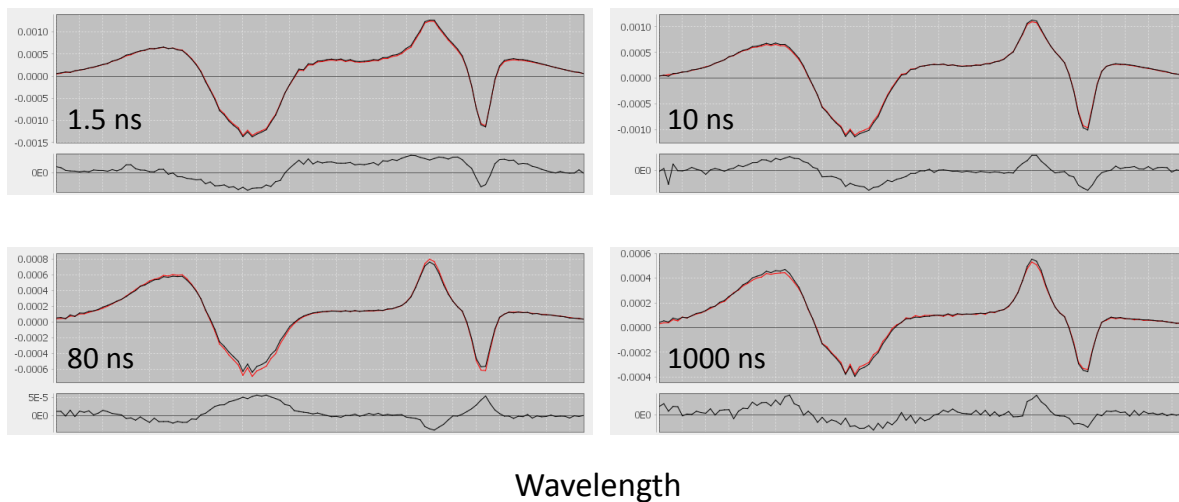


Figure S15. Experimental (black) and fitted (red) nanosecond TRIR spectra of **Re126WWCu^I** at selected time delays. Residuals are shown below the spectra. Conditions as in Figures 6 and 7. The x-axis is calibrated in detector pixels, corresponding to IR-probe wavelength.

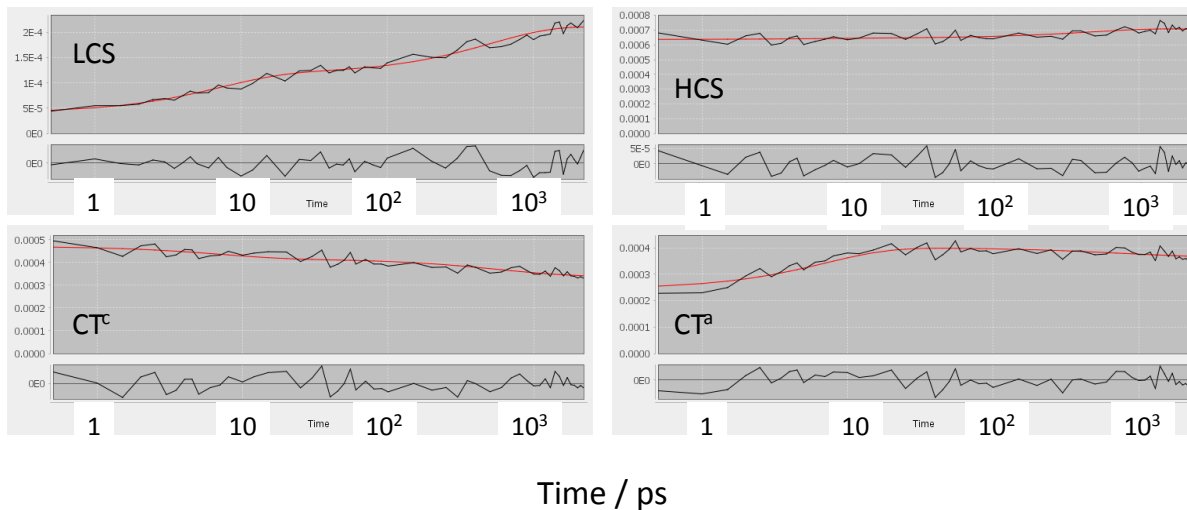


Figure S16. Experimental (black) and fitted (red) time profiles of picosecond TRIR differential absorbance of $\text{Re126WWCu}^{\text{I}}$ measured at maxima of selected IR features. Residuals are shown below the profiles. Conditions as in Figures 6 and 7. The initial CT^{a} rise is due to relaxation.

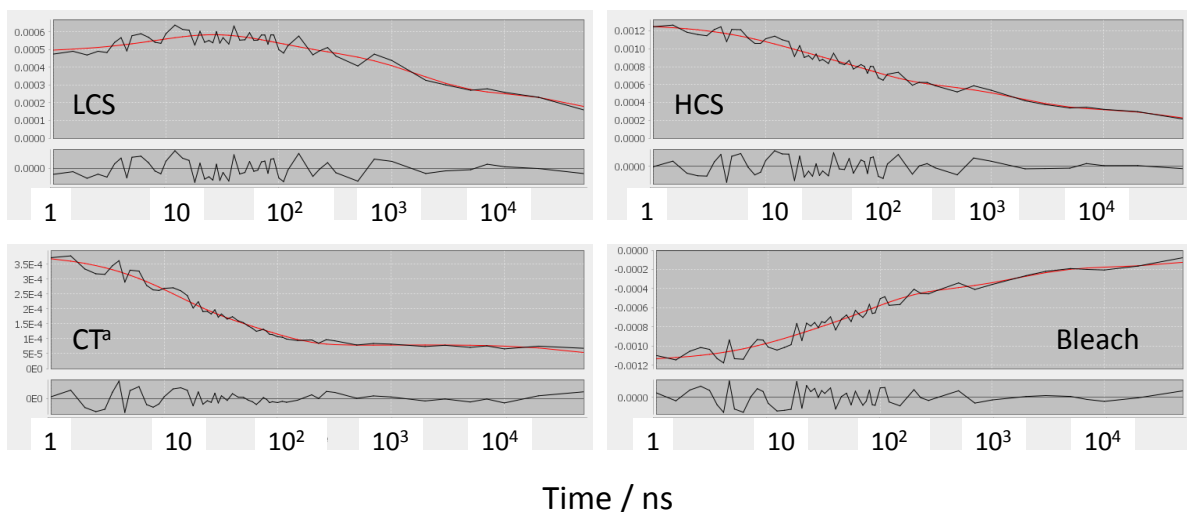


Figure S17. Experimental (black) and fitted (red) time profiles of nanosecond TRIR differential absorbance of $\text{Re126WWCu}^{\text{I}}$ measured at maxima of selected IR features. Residuals are shown below the profiles. Conditions as in Figures 6 and 7. Bleach profile measured at 2028 cm^{-1} .

References

1. Takematsu, K.; Williamson, H.; Blanco-Rodríguez, A. M.; Sokolová, L.; Nikolovski, P.; Kaiser, J. T.; Towrie, M.; Clark, I. P.; Vlček, A., Jr.; Winkler, J. R.; Gray, H. B., Tryptophan-accelerated electron flow across a protein-protein interface. *J. Am. Chem. Soc.* **2013**, *135*, 15515–15525.
2. Takematsu, K.; Williamson, H.; Nikolovski, P.; Kaiser, J. T.; Pospíšil, P.; Towrie, M.; Heyda, J.; Hollas, D.; Záliš, S.; Gray, H. B.; Vlček, A.; Winkler, J. R., Two tryptophans are better than one in accelerating electron flow through a protein. *ACS Cent. Sci.*, *submitted*.
3. Horng, M. L.; Gardecki, J. A.; Papazyan, A.; Maroncelli, M., Subpicosecond Measurements of Polar Solvation Dynamics: Coumarin 153 Revisited. *J. Phys. Chem.* **1995**, *99*, 17311-17337.
4. Blanco-Rodríguez, A. M.; Busby, M.; Ronayne, K. L.; Towrie, M.; Grădinaru, C.; Sudhamsu, J.; Sýkora, J.; Hof, M.; Záliš, S.; Di Bilio, A. J.; Crane, B. R.; Gray, H. B.; Vlček, A., Jr., Relaxation Dynamics of $[\text{Re}^{\text{I}}(\text{CO})_3(\text{phen})(\text{HisX})]^+$ (X = 83, 107, 109, 124, 126) *Pseudomonas aeruginosa* Azurins. *J. Am. Chem. Soc.* **2009**, *131*, 11788-11800.